Research Article Vol. 59, No. 28 / 1 October 2020 / Applied Optics 8839

applied optics

Optics mounting and alignment for the central optical bench of the dual cavity enhanced light-shining-through-a-wall experiment ALPS II

Li-Wei Wei,* Kanioar Karan, and Benno Willke

Institut für Gravitationsphysik der Leibniz Universität Hannover and Max Planck Institute for Gravitational Physics (Albert Einstein Institute), Callinstraße 38, D-30167 Hannover, Germany
**Corresponding author: li-wei.wei@aei.mpg.de*

Received 17 July 2020; revised 1 September 2020; accepted 1 September 2020; posted 2 September 2020 (Doc. ID 401346); published 29 September 2020

Any Light Particle Search II (ALPS II) is a light-shining-through-a-wall experiment seeking axion-like particles. ALPS II will feature two 120 m long linear optical cavities that are separated by a wall and support the same photon mode. The central optical bench at the core of the experiment will be equipped with a light-tight shutter and two planar mirrors for the cavities. We show that the mounting concept for ALPS II provides sufficient angular stability and verify that a simple autocollimator assisted alignment procedure for crucial components of the ALPS II optical cavities can lead to the required overlap of the cavity eigenmodes. Furthermore, we show that mounted quadrant photodiodes added to the optical bench can have sufficient stability to maintain this overlap even without a clear line of sight between the two optical cavities. © 2020 Optical Society of America

https://doi.org/10.1364/AO.401346 Provided under the terms of the OSA Open Access Publishing Agreement

1. INTRODUCTION

An axion is a hypothetical particle beyond the standard model of particle physics that emerges as a pseudo Nambu–Goldstone boson from the spontaneous breaking of the proposed Peccei–Quinn symmetry, which is one solution to the strong charge–parity (CP) problem in quantum chromodynamics (QCD) [1–3]. Various experiments have been proposed and carried out to probe the finite coupling between such so-called QCD axions and the photons, predominantly with a mechanism analogous to the Primakoff effect [4], in which a strong magnetic field boosts the very weak axion–photon coupling process [5].

The weakly interacting property of the axions with normal matter makes axions a sound dark matter candidate [6]. Axion-like particles refer to extensions to the axion model that relieves the specific relation between its mass and coupling strength as required by QCD. We will use *axions* to refer to axion-like particles, as experiment-wise they interact with photons in the same manner, and *QCD axions* will be used to refer to axions that fulfill QCD requirements. The main implication for QCD axions in photon-based experiments is that the coupling strength scales with mass. On the one hand, the lower the target mass for the search, the more demanding the experiments generally are to reach QCD axion sensitivity. On the other hand, when axion mass becomes significant, its phase difference to a massless photon also deteriorates search sensitivity.

Some experiments target detecting axions, in the form of photons following the coupling process, of astrophysical origins such as the Sun and the dark matter halo that rely on model-based particle flux estimates [7,8]. In a light-shining-through-a-wall experiment such as Any Light Particle Search II (ALPS II), axions are first produced by a photon source, very few of which are later regenerated into photons [9–11].

As the name suggests, the concept of a light-shining-through-a-wall experiment is fairly straightforward: a flux of photons is directed towards a light-tight opaque wall, and a photo-detector is placed on the other side of the wall waiting to be triggered by any energy pellets that undergo the photon-axion-photon process.

Experiments to date have not been able to detect axions, while increased sensitivity of the searches translates the non-detection of a signal above the noise level into a better constrained upper limit on the axion–two-photon field coupling coefficient $g_{a\gamma\gamma}$ at various mass ranges that in turn contributes to the parameter exclusion plots (see, e.g., Section 111 of the 2018 Review of Particle Physics [12]).

As depicted in Fig. 1, ALPS II is a dual cavity enhanced light-shining-through-a-wall experiment that targets at a search sensitivity on the field coupling coefficient $g_{a\gamma\gamma}$ of 2×10^{-11} GeV^{-1} [13] that intrudes into uncharted parameter space with strong astrophysical favor that hints at a potential detection of axions [14–16].

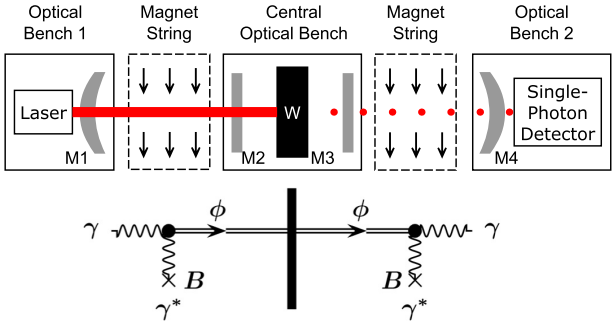

Fig. 1. Schematic and Feynman diagram of the ALPS II experiment, in which γ represents a photon field, γ^* represents a virtual photon field supplied by the magnetic field B, and ϕ is the axion field. M, mirror; W, wall (a light-tight shutter in practice); solid red line, axion-producing photon field; dotted red line, axion-regenerated photon field.

In Section 2, we give an overview of the ALPS II experiment with a stress on optics design and the central optical bench. In Section 3, we present the mounting concepts for the central optical bench in ALPS II, its angular alignment with the use of an autocollimator and long-term stability. In Section 4, we use cavity eigenmode scanning measurements to verify the use of the autocollimator in defining the stringent parallelism required between two reflecting mirror surfaces. In Section 5, we show that the mounted quadrant photodiodes added to the central optical bench also meet the requirements of ALPS II. In Section 6, we conclude our work.

2. ALPS II RESONANT CAVITIES AND THE CENTRAL OPTICAL BENCH

Resonant Fabry–Perot cavities are not unseen in enhancing the sensitivity of experiments that exploit photons. A recent paramount example is the laser interferometric gravitational wave detectors [17,18], in which a power recycling cavity, a signal recycling cavity, and arm cavities are implemented to achieve the unprecedented strain sensitivity that allowed for the observation of the mergers of binary black holes and binary neutron stars [19,20].

The resonant gain of Fabry–Perot cavities is also applicable to a light-shining-through-a-wall experiment, and ALPS II will be the first experiment, to the best of our knowledge, to feature a dual cavity enhanced optical design [5,21]. Referring to Fig. 1, the probability $\mathbb{P}$ of a photon emitted by the laser that undertakes the photon-axion-photon process to appear at the detector is shown to be

$$\mathbb{P} \propto \left[g_{a\gamma\gamma} \cdot \int B \mathrm{d}L_B\right]^4 \left[\beta_{1|2} \cdot \beta_{3|4}\right]$$
$$\approx \left[g_{a\gamma\gamma} \cdot \int B \mathrm{d}L_B\right]^4 \left[\frac{F}{\pi}\right]^2, \quad (1)$$

where $\beta_{1|2}$ is the power build-up factor of the production cavity, $\beta_{3|4}$ is that of the regeneration cavity, and the approximation sign assumes two identical impedance matched cavities of finesse F [22], as discussed in more detail in Appendix A.

Equation (1) indicates the importance of the magnetic field B and its integration over the interaction length L_B of one magnet string, for which ALPS II will use the superconducting dipole magnets from *Hadron-Elektron-Ring-Anlage* (HERA, Hadron Electron Ring Facility) in *Deutsches Elektronen-Synchrotron* (DESY, German Electron Synchrotron) Hamburg. The dipole magnets will form two strings, each consisting of 12 magnets with 8.8 m effective length (i.e., $L_B \approx 105.6$ m) and 5.3 T magnet field [23] and encompassed by an $L_c \approx 120$ m long plano-concave Fabry–Perot cavity.

We refer to these cavities as the (axion-) production cavity and the (photon-) regeneration cavity, which consist of M1 and M2 and M3 and M4, in Fig. 1, respectively. ALPS II will use an infrared (IR) laser at a 1064 nm wavelength for axion production, thereby importing many readily available techniques and technologies from the gravitational wave detectors, e.g., the high-power single-frequency laser sources and the high-quality high-reflection mirror coatings. M1 will have a higher transmissivity than M2, such that the production cavity is over-coupled to maximize the probability $\mathbb{P}$ for a given finesse. Similarly, when only one detector is implemented (as in ALPS II), for the regeneration cavity, one can slightly increase the transmissivity of the mirror that is on the detector side.

ALPS II calls for an aggressive combined resonant gain of 2×10^8 ($\beta_{1|2} = 5000$ and $\beta_{3|4} = 40{,}000$ have been anticipated in the ALPS II technical design report [13]) in the probability $\mathbb{P}$ from the dual optical cavity configuration. In other words, the dual resonance cavities optically boost the search sensitivity in $g_{a\gamma\gamma}$ by more than two orders of magnitude (fourth root of 2×10^8 is ≈ 119).

An ALPS II prototyping experiment with a reduced cavity length of 9.2 m has demonstrated a finesse of $101{,}300 \pm 500$ [24] that approaches the goal on $\beta_{3|4}$ called for by ALPS II. The losses in the ALPS II cavities are expected to be dominated by the surface quality of the cavity mirrors. Given the scatter loss estimated from the delivered cavity mirrors, $\beta_{3|4} \approx 16{,}000$ is expected for the initial science phase of ALPS II [25].

In addition to a probability $\mathbb{P}$ that is defined by the magnet strings and the cavity configurations, the input laser power, the search time, the efficiency, and the dark count rate of the detector also affect the eventual search sensitivity of ALPS II. The targeted search sensitivity of $g_{a\gamma\gamma} = 2 \times 10^{-11}$ GeV^{-1} is equal to a flux of about two photons per day at the detector in the ALPS II design.

In terms of optics, one of the main challenges is to ensure that the two Fabry–Perot cavities across the wall support the very same spatial-temporal photon mode, a task that can be broken down into the control on (1) the longitudinal degree of freedom that concerns laser frequencies and cavity lengths and (2) the transverse degrees of freedom that concern the spatial profile of the cavity eigenmodes as defined by cavity geometry.

Due to the extremely low regenerated photon flux of the experiment, it is practically impossible to use photons that resemble the axion-regenerated photons to interrogate the regeneration cavity, as the shot noise of the interrogating photons simply overwhelms the axion-regenerated photon signal.

Two types of single-photon detectors will be implemented sequentially in ALPS II, each of which requires a specialized

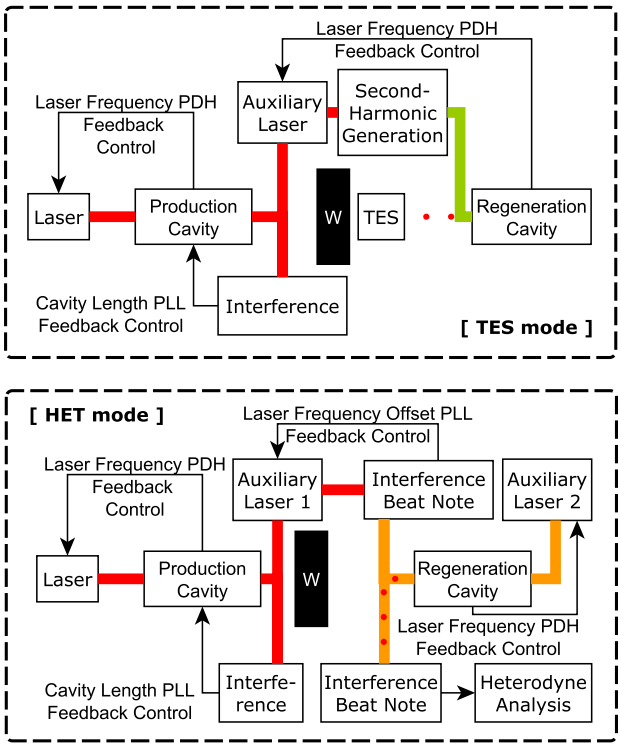

Fig. 2. ALPS II control schemes on lasers and optical cavities for the TES mode and the HET mode. PDH, Pound–Drever–Hall laser-frequency stabilization technique [28,29].

control technique for its own on the longitudinal degree of freedom. Single-photon detection will be done in ALPS II with a transition edge sensor (TES mode) [26] or coherent heterodyne detection (HET mode) [27]. The detection concepts along with the dedicated control schemes are illustrated in Fig. 2.

In TES mode, a second-harmonic field in green will be used to interrogate the regeneration cavity. Phase-frequency relation is governed by the harmonic relation between the IR and green photons. The TES has a typical energy resolution of $\approx 10\%$ that suffices in differentiating the photons of these two colors. Green photons will still be filtered to reduce the green photon induced counting events and to avoid detector saturation issues.

In the HET mode, an offset IR field will be used to interrogate the regeneration cavity. The optical-frequency offset will be a multiple of the free spectral range of the cavities. A heterodyning beat signal between this offset IR field and the regenerated IR field following a photon-axion-photon process is then demodulated at the offset frequency to give associated photon counts.

Either the TES mode or the HET mode embodies optics design details that merit its own account. In this paper, we are instead focusing on the transverse degrees of freedom of the cavity eigenmodes. Regardless of the detection mode, the spatial control of the photon modes in ALPS II relies on the central optical bench that sits at the core of the experiment, as illustrated in Fig. 1 and enlarged in Fig. 3, with the inclusion of quadrant photodiodes.

In a plano-concave linear cavity, the waist of the eigenmode is located on the planar mirror, and the propagation axis of the eigenmode is defined by the orientation of the planar mirror.

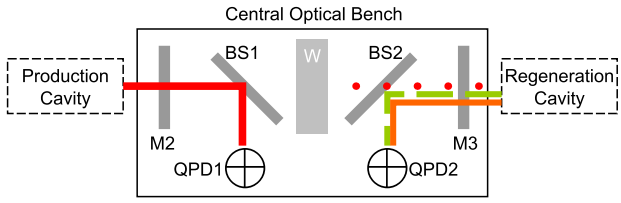

Fig. 3. Schematic of the ALPS II central optical bench. BS, beam-splitter; QPD, quadrant photo-detector.

That is, as long as the two reflecting planar mirrors of the two cavities are parallel, so are the optical axes of their eigenmodes.

Once parallelism is ensured between the planar mirrors, the remaining transverse degree of freedoms of the cavity eigenmodes, i.e., the lateral positions of the waists on the planar mirrors, are defined by the curved (concave) mirrors.

The task here is then to center the eigenmodes to the bore of the magnet strings with limited aperture; clipping loss needs to be minimized to achieve high finesse cavity operation. More important is the alignment of the two eigenmodes such that they are spatially overlapped.

ALPS II aims at achieving $\approx 99\%$ power overlap between the eigenmodes of the production cavity and the regeneration cavity in the transverse degrees of freedom. A tolerance allocation is defined in terms of power percentage ϵ scattered into the high-order modes on a perturbative basis as [30–32]

$$\begin{aligned}\epsilon \equiv \epsilon_1 + \epsilon_2 &\approx \frac{|U_1|^2}{|U_0|^2} + \frac{|U_2|^2}{|U_0|^2} \\ &\approx \left(\frac{\delta\alpha_{\mathrm{eig}}}{\theta_{0,\mathrm{eig}}}\right)^2 + \left(\frac{\delta x_{\mathrm{eig}}}{w_{0,\mathrm{eig}}}\right)^2 + \left(\frac{\delta z_{0,\mathrm{eig}}}{2\cdot z_R}\right)^2 + \left(\frac{\delta w_{0,\mathrm{eig}}}{w_{0,\mathrm{eig}}}\right)^2 \\ &\le \left(\frac{5\ \mu\mathrm{rad}}{56.5\ \mu\mathrm{rad}}\right)^2 + \left(\frac{0.1\ \mathrm{mm}}{6\ \mathrm{mm}}\right)^2 + \left(\frac{1\ \mathrm{m}}{2\cdot 106\ \mathrm{m}}\right)^2 + \left(\frac{0.2\ \mathrm{mm}}{6\ \mathrm{mm}}\right)^2 \\ &\approx 0.78\% + 0.28\% + 0.0022\% + 0.11\% \approx 1.17\%,\end{aligned} \tag{2}$$

where $\delta\alpha_{\mathrm{eig}}$ is the relative angle, δx_{eig} is the relative lateral position, $\delta z_{0,\mathrm{eig}}$ is the relative axial position, and $\delta\omega_{0,\mathrm{eig}}$ is the waist radius difference between the two cavity eigenmodes; $\theta_{0,\mathrm{eig}}$ is the half-divergence angle, $w_{0,\mathrm{eig}}$ is the waist radius, and z_R is the Rayleigh range of the cavity eigenmodes. The numerical values of the ALPS II cavity parameters are derived with a curved mirror radius of curvature of 214 m $\pm$ 10 m and a cavity length L_c of 120 m.

The latter two terms in Eq. (2), $\delta z_{0,\mathrm{eig}}$ and $\delta\omega_{0,\mathrm{eig}}$, depend on the difference in the radii of curvature of the curved cavity mirrors and the distance between the planar mirrors. We will concentrate on the first two terms of Eq. (2), which state the requirements on the parallelism of the planar mirrors and on the lateral displacement of the cavity eigenmodes.

Figure 4 shows the schematic of the table-top optics setup for the assembly and verification purposes of the ALPS II central optical bench. The first task is to ensure strict parallelism between mirrors M2 and M3 and to demonstrate its long-term stability. The second task is to install the beam-splitters (BSs) and have the quadrant photodiodes aligned to a predefined

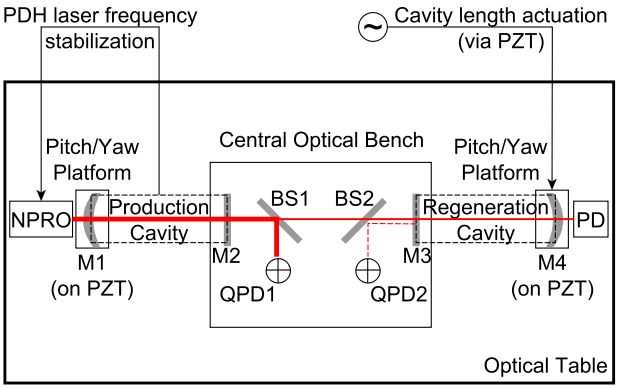

Fig. 4. Schematics of the optics setup for the tests. NPRO, non-planar ring oscillator; PD, photo-detector; PZT, piezoelectric transducer.

optical axis. In the following, we will show more details to the mounting concepts for the components on the central optical bench and use the table-top setup to validate it with respect to ALPS II requirements discussed in Eq. (2).

3. CENTRAL OPTICAL BENCH MIRROR MOUNTS AND AUTOCOLLIMATOR ASSISTED ALIGNMENT

Referring to Fig. 4, two 1 m linear cavities, whose planar mirrors are mounted on a realistic ALPS II central optical bench, are set up to test two mounting concepts. Mirror M3 is installed to a commercial high-stability mount (Thorlabs Polaris K1T) for 1 in. circular optics, and mirror M2 is a cuboid optics (50 mm × 50 mm × 10 mm) that is clamped to the optical bench with a compact Π-shaped frame and spring-loaded ball-tip screws, as shown in Fig. 5. BS1 and BS2 are also cuboid optics (50 mm × 50 mm × 10 mm) directly clamped to the optical bench.

We note that the Π-shaped clamping frame is tested for its potential advantage of a smaller footprint, which may be limited in the ALPS II experiment due to various boundary conditions. In addition, the use of clamped cuboid optics allows for the possibility to tackle the stringent angular requirements in Eq. (2) by means of precise optics and breadboard treatment. In the Π-shaped clamp concept, strictly right-angled cuboid optics and

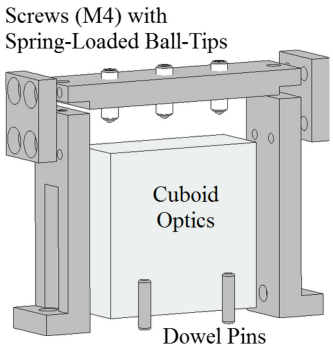

Fig. 5. Π-shaped clamping frame with spring-loaded ball-tip screws. The force exerted by each screw is specified to be 8.5 N and 14 N at the beginning and the end of its 0.8 mm travel range.

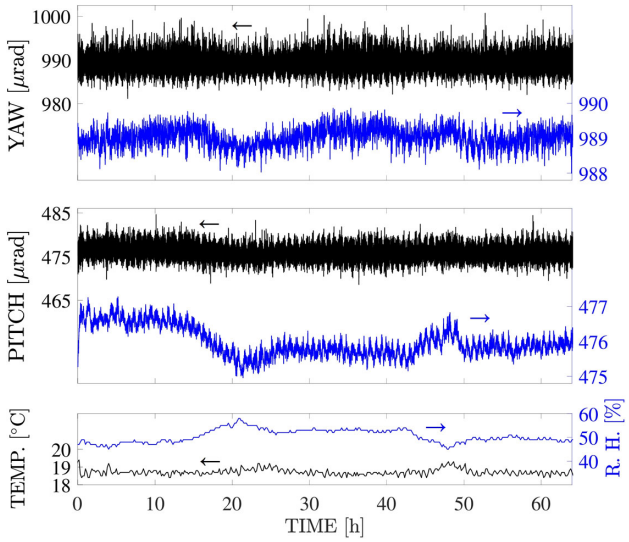

Fig. 6. Autocollimator measurement time series on the angle between a Π-clamped rectangular mirror and a commercial high-stability mount. Raw angle (yaw/pitch) measurements are sampled at ≈ 110 ms intervals and plotted in black using the left y axis. Moving-averaged curves with 1000 data samples are plotted in blue using the y axes on the right for better correlation visibility. The temperature (in black) and relative humidity (R.H., in blue) data are sampled every 10 min. A strong correlation of −0.75 (Pearson correlation coefficient) exists between the pitch angle (averaged to 10 min sampling period) and relative humidity, to be compared with the correlation of −0.17 between the yaw angle and relative humidity. The correlation to temperature is −0.05 for yaw and −0.14 for pitch. The correlation calculations are not optimized with phase shifts.

an ultra-planar breadboard with dowel pins (or grooves) may be used to define the parallelism between the planar mirrors. As there are no movable components in such a symmetric structure, drifts due to environmental fluctuations are also expected to be minimized.

An autocollimator (Trioptics TriAngle TA 300-57) with 300 mm focal length and 50 mm aperture is firstly used to test the long-term stability of these two mounts by registering their relative angle. The resultant time series are shown in Fig. 6, and their histograms in Fig. 7. The standard deviation σ is 1.03 μrad for yaw and 0.89 μrad for pitch.

Since these measurements are not performed in a well-protected quiet environment (in contrast to ALPS II), we pay attention to the moving-averaged curves. The 2 min moving-averaged time series show a stability of ≈ 2 μrad peak-to-peak per degree of freedom, in yaw and in pitch, which is sufficient for the requirement of ALPS II. With a temperature fluctuation of ≈ 1 K peak-to-peak during the measurement, we can infer a thermal-angular coupling coefficient of ≈ 2 μrad/K in pitch, which is comparable to the manufacturer thermal cycle data of ≈ 2 μrad/K (Thorlabs Polaris K1T) and better than the ≈ 4 μrad/K of a previously reported mounting scheme featuring similar commercial mounts [33]. Moreover, we note also the strong correlation between pitch angle and relative humidity, while ALPS II will be operating in vacuum.

The two planar cavity mirrors are then set to be parallel using the autocollimator. We note that due to the wedge angle

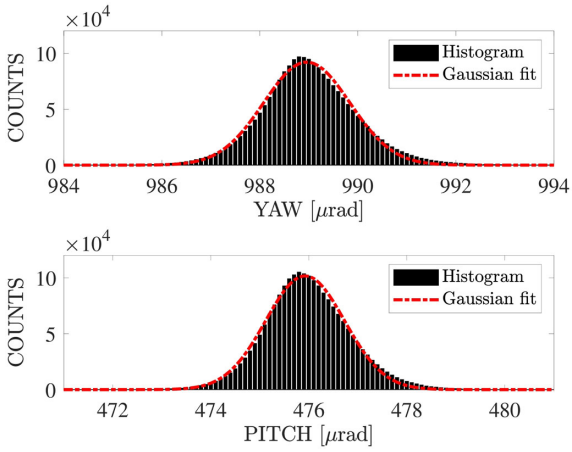

Fig. 7. Histograms of the raw angle measurements in Fig. 6. The bin width is 0.1 μrad.

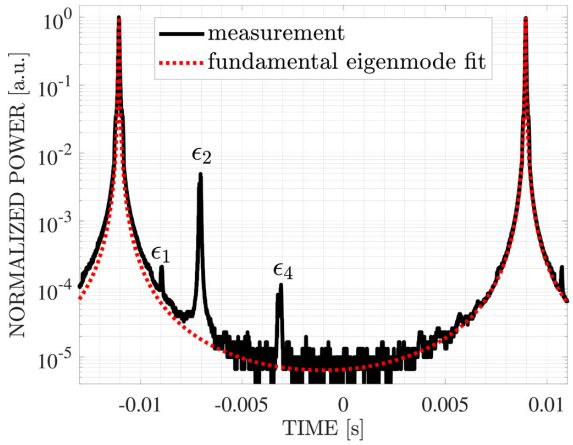

Fig. 8. Cavity eigenmode scan measurement result. The higher-order-mode spacing corresponds to ≈2 ms in the scan. The higher-order-mode spacing of the test cavities is ≈0.1FSR.

(≈ 22 μrad for M2 and ≈ 46 μrad for M3) in the planar mirrors used for the test, the parallelism is slightly detuned according to double-pass autocollimator measurements and simple geometrical optics calculations.

4. MIRROR PARALLELISM VERIFICATION WITH CAVITY EIGENMODE SCANS

The two curved mirrors, with radii of curvature of 10 m, are installed to form two 1 m long test optical cavities using the central optical bench prepared in the described manner. The resultant Rayleigh range, the waist radius, and the half-divergence angle of the plano-concave test cavities of

$$z_R = 3\ \text{m}, \quad \omega_{0,\text{eig}} = 1008\ \mu\text{m}, \quad \text{and} \quad \theta_{0,\text{eig}} = 336\ \mu\text{rad} \tag{3}$$

are used for the analysis of the presented measurements.

The curved mirrors are placed in three-axis piezoelectric transducer (PZT) mirror mounts that are in turn placed on pitch and yaw platforms (Thorlabs PY004/M). Due to the plano-concave cavity geometry, angular tilts of the curved mirrors correspond to lateral translations of the cavity eigenmodes on the planar mirrors. The platforms are used for coarse adjustments to not saturate the fine-tuning range provided by the PZT mirror mounts.

For testing purposes, there is no wall on the central optical bench, and only one IR laser is used. As illustrated in Fig. 4, an non-planar ring oscillator (NPRO) laser at 1064 nm wavelength (Coherent Mephisto) is frequency-stabilized to the length of the production cavity in the fundamental eigenmode. The length of the regeneration cavity is actuated by more than a free spectral range, and, by analyzing the transmitted power through the regeneration cavity with respect to the actuated cavity length, the transmitted field of the production cavity is decomposed in terms of the eigenmodes of the regeneration cavity. The eigenmode contents can then be translated into angular and lateral movements according to Eq. (2).

The three PZT actuators (Physik Instrumente S-315.10) for the curved mirrors form a triangular constellation and are controlled with matrix amplifiers. In order to ensure a pure piston motion along the optical axis so that no spurious higher-order modes are introduced during the length scanning of the regeneration cavity, the PZT actuators together with the matrix amplifiers are tuned and calibrated using the autocollimator.

The yaw and pitch of the curved mirror of the regeneration cavity are tuned to minimize the order-one eigenmode content in cavity transmission over a cavity length scan. By doing so, we cross out the term coming from lateral misalignment in Eq. (2), and the residual is attributed to angular misalignment that relates to the parallelism between the two planar mirrors. It is convenient to combine Eqs. (2) and (3) to project the ALPS II requirements to first-order eigenmode content (ϵ_1) equivalent to

$$\epsilon_1 \le \left(\frac{5\ \mu\text{rad}}{336\ \mu\text{rad}}\right)^2 \approx 2.2 \times 10^{-4} \tag{4}$$

for the angular degree of freedom, where the lateral degree of freedom is assumed to be nulled after the minimization procedure with the curved mirrors. The second-order eigenmode content (ϵ_2) equivalent due to finite relative waist location mismatch is also calculated for sanity check as

$$\epsilon_2 \approx \left(\frac{0.5\ \text{m}}{2 \cdot 3\ \text{m}}\right)^2 \approx 0.007. \tag{5}$$

A photodiode with a transimpedance preamplifier is used for power measurements of the field transmitted by the regeneration cavity while scanning its length, followed by two subsequent 100 V/V (40 dB) amplifier stages in series. The three voltage outputs (+0 dB, +40 dB, +80 dB), with different noise floors and saturation levels, are combined to form the eigenmode scanning measurement shown in Fig. 8. We are able to reduce the order-one eigenmode content ϵ_1 to $\approx 2.1 \times 10^{-4}$, which meets the ALPS II requirement in Eq. (4). We note that the residual spurious ϵ_1 content from the length scan is $\approx 3.6 \times 10^{-5}$ after the calibration using the autocollimator.

The measured order-two eigenmode content is ≈0.005, which is lower than the value estimated in Eq. (5). This may be partly due to a larger radius of curvature of the mirrors

than specified, as well as higher clipping loss experienced by higher-order modes on a photodiode with finite aperture.

The finesse of the test regeneration cavity calculated from the least-squares fit of the eigenmode scan in Fig. 8 is 430, while the expected value from mirror coating specifications is 623. Despite the deteriorated finesse from expectation, the test regeneration cavity nevertheless suffices as a discriminator for ALPS II central optical bench alignment requirements.

The discussed assembly procedure therefore complies with the ALPS II requirements in defining the parallelism of the planar mirrors that governs the angular degree of freedom of the cavity eigenmodes. We recall that the assembly procedure is assisted with an autocollimator, which has its roles in defining the parallelism between the two reflection planar mirror surfaces, in correcting for the wedge angle in the common path of photons and axion and in calibrating the PZT-mounted curved mirrors for true piston motion. Our study explicitly verifies the applicability of autocollimators in many aspects in the preparation of the ALPS II central optical bench and directly leads to the two implications as follows.

First, instead of using a cavity setup to walk through all four degrees of freedom (angular and lateral in the vertical and horizontal planes) and minimize the ϵ_1 content in the eigenmode scan to achieve precise alignment, one can use the autocollimator to decouple the angular and lateral degrees of freedom, which largely streamlines the alignment task. The use of an autocollimator provides a credible angular alignment reference, and its almost real-time signed response appears to be rather essential in practice for the alignment task even when a high-stability commercial mirror mount (Thorlabs Polaris K1T) is used, which has a specified mechanical resolution of 5 μrad (typical) and 2 μrad (achievable).

Second, to ensure that the refraction of photons is nulled in between the two cavities, one option that appears costly is to place stringent specifications on the residual wedge angle of the planar mirrors, while in our tests we use the autocollimator to address the wedge angle, and the results are plausibly supported by the sufficiently low ϵ_1 content in the cavity eigenmode scan. Obviously, in ALPS II, one cannot detune the parallelism between the two planar mirrors, but it remains a possibility to cherry-pick (circular) optics and clock them with respect to their wedge angles in a way that the refraction is nulled.

5. ADJUSTABLE AND LOCKABLE QUADRANT PHOTODIODE MOUNT

ALPS II anticipates the use of quadrant photodiodes mounted to the central optical bench as the lateral alignment reference of the cavity eigenmodes. The positional information of the cavity eigenmodes derived from the quadrant photodiodes can then either be used as the input of an active stabilization system, or simply as the monitoring signal for the calibration of the probability $\mathbb{P}$ in Eq. (1) when the shutter is closed.

Referring to Fig. 3, the lateral position of the production cavity eigenmode is always sensed at the 1064 nm IR wavelength. For the regeneration cavity eigenmode in TES mode, the second-harmonic field at the 532 nm green wavelength is used, while, in the HET mode, the offset IR wavelength is used.

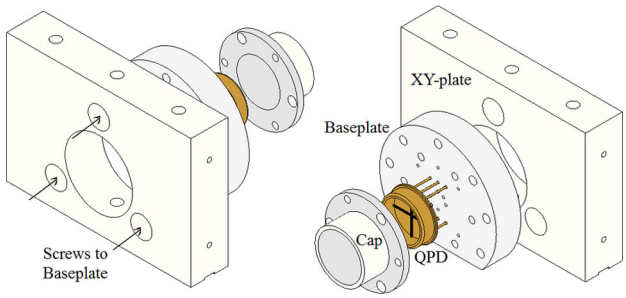

Fig. 9. Mounted quadrant photodiode assembly. The quadrant photodiode is sandwiched between a baseplate and a cap with screws. The baseplate translates on the XY plate for alignment purposes and is fixed once aligned.

Due to the large waist radius of the ALPS II cavity eigenmodes in comparison to the typical active aperture of quadrant photodiodes, despite the use of beam reducing optics, it is practical to center the quadrant photodiodes to the impinging laser beam to minimize clipping and scattering. Stability remains nevertheless the most important factor for the mounted quadrant photodiodes.

We use a mounting concept derived from the Advanced Virgo laser power stabilization photodiode module, where centering of the photodiode to the laser beam is crucial in reducing the spurious power noise resulting from the coupling between laser beam pointing fluctuation, finite photodiode active aperture, and a moderate beam spot radius that avoids exceeding current density in the photodiode for high photo-current operation [18,34,35]. The adaption for ALPS II is illustrated in Fig. 9. For our tests, silicon quadrant photodiodes with 7.98 mm active diameter (First Sensor QP50-6, TO-8 package) are used.

Since the distances between the quadrant photodiodes and the planar cavity mirrors are much smaller than the Rayleigh range of the cavity eigenmodes, the laser beam spot radii on the quadrant photodiodes are approximated to be $\omega_{0,\mathrm{eig}} = 1008$ μm for the mutual stability test that follows.

The mutual stability of the mounted quadrant photodiodes is assessed by sending an IR laser to the central optical bench (see Fig. 4), whose positional information on the quadrant photodiodes is registered and compared, as shown in Fig. 10. Over the course of more than 100 h, the differential peak-to-peak drifts measured with the two quadrant photodiode modules are 35.9 μm in ΔX and 31.2 μm in ΔY, which are sufficient for the tolerance given in Eq. (2). The air temperature and relative humidity time series are also shown in Fig. 10. In ALPS II, the central optical bench will be operated in vacuum such that improved stability of these mounted quadrant photodiodes is to be expected.

Based on the cavity eigenmode scan measurement shown in Fig. 8, controlled tilts are introduced to the curved mirror M1 that can be quantified by the eigenmode content ϵ_1 by means of Eq. (2). The corresponding lateral movement of the fundamental production cavity eigenmode δx_{eig} is measured with both quadrant photo-detector (QPD1) and QPD2 and compared to its decomposition in terms of the eigenmode content of the regeneration cavity that is scanned in length. The results are

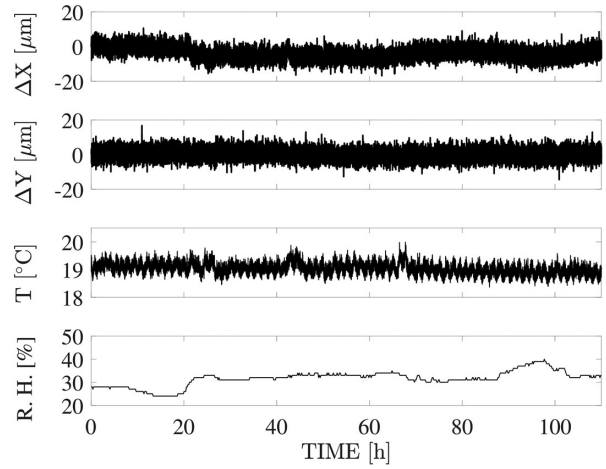

Fig. 10. Mounted quadrant photodiode modules reading comparison. ΔX refers to the positional readout difference in the horizontal plane, and ΔY is the vertical plane; ΔX and ΔY are zeroed to their mean values in the plot for better visualization. Air temperature and relative humidity are also shown to signify potentially increased stability of the setup when operating in vacuum.

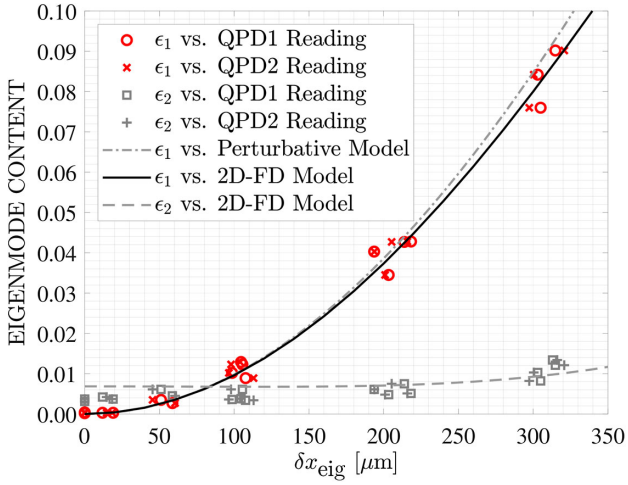

Fig. 11. Eigenmode content versus quadrant photodiode readings with intentional tilts introduced to curved mirror M1. $\delta x_{\mathrm{eig}} = [\mathrm{X}^2 + \mathrm{Y}^2]^{1/2}$, and the origins of quadrant photodiode readings X and Y are defined with respect to the minimal ϵ_1 measured in the cavity eigenmode scan. The same ϵ measurements in the y axis are plotted with respect to the two quadrant photodiode measurements as the x axis. The perturbative model curve uses Eq. (2) with $\omega_{0,\mathrm{eig}} = 1008$ μm.

shown in Fig. 11 together with the expected relation between δx_{eig} and the eigenmode contents ϵ_1 and ϵ_2.

We are mostly concerned by ϵ_1, while ϵ_2 is also measured for a better understanding of the system. In addition to the perturbative relation in Eq. (2), two-dimensional finite-difference (2D-FD) calculations of

$$\epsilon_k = \sum_{i,j\in\mathbb{N}}^{i+j=k} \left\{ \iint U_{00}(x, y, 0) \cdot U_{ij}^*(x + \Delta_{\mathrm{eig}}, y, \delta z_{0,\mathrm{eig}}) \mathrm{d}x\mathrm{d}y \right\}, \tag{6}$$

which takes into account both the relative axial position and the relative lateral position contribution to ϵ_k, are also plotted for a more accurate account, where $U_{ij}(x, y, z)$ denotes the field of a Hermite–Gaussian beam of order (i, j) [36]. The two models for ϵ_1 agree almost perfectly for $\delta x_{\mathrm{eig}} \lesssim 150$ μm or $\epsilon_1 \lesssim 2\%$. ALPS II is anticipated to work with sub-percent ϵ_1, for which the perturbative account of Eq. (2) is valid. For larger eigenmode displacements, despite measurement uncertainty, the 2D-FD model better describes the data. A slight increase in ϵ_2 is also observed and explained by the 2D-FD calculation when the lateral movement becomes large.

Across the range of the measurements shown in Fig. 11, up to ≈ 20 μm departure is observed between the data points and the 2D-FD model curve, which coincides with the mounted quadrant photodiode stability measurement noise seen in Fig. 10 and complies with the ALPS II requirements outlined in Eq. (2).

In addition to the angular degree of freedom of the eigenmode of a plano-concave cavity, which is defined by the planar mirror as discussed in the previous section, quadrant photodiodes are now also introduced to track the lateral degree of freedom. The results shown in Figs. 10 and 11 justify the stability of the mounted quadrant photodiode assembly and the tracking concept for the ALPS II experiment.

6. CONCLUSION

We show that the proposed optics mounting and alignment concept for the central optical bench fulfill the requirements of ALPS II, which anticipates the exploitation of aggressive resonant optical gain to achieve its scientific goal in an axion search. An off-the-shelf high-stability optics mount and a custom-made clamping mount for compactness have both been shown to meet ALPS II requirements. The autocollimator-based alignment concept is verified with an actual ALPS-II-like dual cavity setup, where cavity eigenmode scanning results qualify ALPS II specifications. An adjustable and lockable quadrant photodiode mounting design is also shown and tested to meet the requirements.

ALPS II is the leading light-shining-through-a-wall experiment that is currently being implemented for dark matter searches. The results presented here on the stability and the accuracy of the alignment of the cavities are a prerequisite to correctly interpret the outcome of the ALPS II experiment and provide information on the axion–two-photon field coupling constant $g_{a\gamma\gamma}$, which is of particular importance for science communities in particle physics, astrophysics, astroparticle physics, and the like.

APPENDIX A

Referring to Fig. 1, when on resonance and at steady-state, using the formulation in Ref. [36], the field amplitude of the laser E_L and the circulating field between mirrors M1 and M2, $E_{1|2}$, are related by

$$E_{1|2} = t_1 \cdot E_L + \sigma_{1|2} \cdot E_{1|2}, \tag{A1}$$

where

$$\sigma_{1|2} = r_1 \cdot r_2 \cdot \exp\left[-\alpha_{1|2} \cdot 2L_c\right] \tag{A2}$$

denotes the fraction of amplitude that remains after one cavity round-trip, t_i is the amplitude transmission coefficient, r_i is the amplitude reflection coefficient of mirror Mi, and $\exp[-\alpha_{1|2} \cdot 2L_c]$ is the intra-cavity loss in one round-trip. It then follows that

$$\sqrt{\beta_{1|2}} \equiv \frac{E_{1|2}}{E_L} = \frac{t_1}{1-\sigma_{1|2}} \approx \frac{t}{1-r^2} = \frac{1}{t} \approx \sqrt{\frac{F}{\pi}}, \quad \textbf{(A3)}$$

in which we introduce the cavity power build-up factor β, and the first approximation sign assumes a loss-less ($t_i^2 = T_i = 1 - R_i = 1 - r_i^2$ and $\alpha_0 = 0$) impedance matched ($t_1 = t_2 = t$, $r_1 = r_2 = r$) cavity as in Eq. (1).

In a similar fashion, the elementary axion-regenerated electromagnetic field E_R that traverses the magnet string of the regeneration cavity and arrives at mirror M4, the circulating field $E_{3|4}$ between mirrors M3 and M4, and the transmitted cavity field E_D via mirror M4 that is to be detected, are related by

$$E_{3|4} = E_R + \sigma_{3|4} \cdot E_{3|4},\ E_D = t_4 \cdot E_{3|4}, \quad \textbf{(A4)}$$

based on which it can be shown that

$$\sqrt{\beta_{3|4}} \equiv \frac{E_D}{E_R} = \frac{t_4}{1-\sigma_{3|4}}. \quad \textbf{(A5)}$$

We note that t_4 is to be replaced by t_3 when the detector is placed next to mirror M3 and that ALPS II anticipates cavity impedance settings that allow for $\beta > F/\pi$.

Funding. Deutsche Forschungsgemeinschaft (WI 1643/2-1); Volkswagen Foundation.

Disclosures. The authors declare no conflicts of interest.

REFERENCES

1. R. D. Peccei and H. R. Quinn, "Constraints imposed by CP conservation in the presence of pseudoparticles," Phys. Rev. D **16**, 1791–1797 (1977).
2. S. Weinberg, "A new light boson?" Phys. Rev. Lett. **40**, 223–226 (1978).
3. F. Wilczek, "Problem of strong p and t invariance in the presence of instantons," Phys. Rev. Lett. **40**, 279–282 (1978).
4. H. Primakoff, "Photo-production of neutral mesons in nuclear electric fields and the mean life of the neutral meson," Phys. Rev. **81**, 899 (1951).
5. P. Sikivie, D. B. Tanner, and K. van Bibber, "Resonantly enhanced axion-photon regeneration," Phys. Rev. Lett. **98**, 172002 (2007).
6. P. Arias, D. Cadamuro, M. Goodsell, J. Jaeckel, J. Redondo, and A. Ringwald, "WISPy cold dark matter," J. Cosmol. Astropart. Phys. **2012**, 013 (2012).
7. V. Anastassopoulos, S. Aune, K. Barth, A. Belov, H. Bräuninger, G. Cantatore, J. M. Carmona, J. F. Castel, S. A. Cetin, F. Christensen, J. I. Collar, T. Dafni, M. Davenport, T. A. Decker, A. Dermenev, K. Desch, C. Eleftheriadis, G. Fanourakis, E. Ferrer-Ribas, H. Fischer, J. A. García, A. Gardikiotis, J. G. Garza, E. N. Gazis, T. Geralis, I. Giomataris, S. Gninenko, C. J. Hailey, M. D. Hasinoff, D. H. H. Hoffmann, F. J. Iguaz, I. G. Irastorza, A. Jakobsen, J. Jacoby, K. Jakovčić, J. Kaminski, M. Karuza, N. Kralj, M. Krčmar, S. Kostoglou, C. Krieger, B. Lakić, J. M. Laurent, A. Liolios, A. Ljubičić, G. Luzón, M. Maroudas, L. Miceli, S. Neff, I. Ortega, T. Papaevangelou, K. Paraschou, M. J. Pivovaroff, G. Raffelt, M. Rosu, J. Ruz, E. R. Chóliz, I. Savvidis, S. Schmidt, Y. K. Semertzidis, S. K. Solanki, L. Stewart, T. Vafeiadis, J. K. Vogel, S. C. Yildiz, K. Zioutas, and C. A. S. T. Collaboration, "New CAST limit on the axion–photon interaction," Nat. Phys. **13**, 584–590 (2017).
8. T. Braine, R. Cervantes, N. Crisosto, N. Du, S. Kimes, L. J. Rosenberg, G. Rybka, J. Yang, D. Bowring, A. S. Chou, R. Khatiwada, A. Sonnenschein, W. Wester, G. Carosi, N. Woollett, L. D. Duffy, R. Bradley, C. Boutan, M. Jones, B. H. LaRoque, N. S. Oblath, M. S. Taubman, J. Clarke, A. Dove, A. Eddins, S. R. O'Kelley, S. Nawaz, I. Siddiqi, N. Stevenson, A. Agrawal, A. V. Dixit, J. R. Gleason, S. Jois, P. Sikivie, J. A. Solomon, N. S. Sullivan, D. B. Tanner, E. Lentz, E. J. Daw, J. H. Buckley, P. M. Harrington, E. A. Henriksen, and K. W. Murch, "Extended search for the invisible axion with the axion dark matter experiment," Phys. Rev. Lett. **124**, 101303 (2020).
9. K. Ehret, M. Frede, S. Ghazaryan, M. Hildebrandt, E.-A. Knabbe, D. Kracht, A. Lindner, J. List, T. Meier, N. Meyer, D. Notz, J. Redondo, A. Ringwald, G. Wiedemann, and B. Willke, "New ALPS results on hidden-sector lightweights," Phys. Lett. B **689**, 149–155 (2010).
10. J. Redondo and A. Ringwald, "Light shining through walls," Contemp. Phys. **52**, 211–236 (2011).
11. R. Ballou, G. Deferne, M. Finger, M. Finger, L. Flekova, J. Hosek, S. Kunc, K. Macuchova, K. A. Meissner, P. Pugnat, M. Schott, A. Siemko, M. Slunecka, M. Sulc, C. Weinsheimer, and J. Zicha, "New exclusion limits on scalar and pseudoscalar axionlike particles from light shining through a wall," Phys. Rev. D **92**, 092002 (2015).
12. Particle Data Group, "Review of particle physics," Phys. Rev. D **98**, 030001 (2018).
13. R. Bähre, B. Döbrich, J. Dreyling-Eschweiler, S. Ghazaryan, R. Hodajerdi, D. Horns, F. Januschek, E. A. Knabbe, A. Lindner, D. Notz, A. Ringwald, J. E. von Seggern, R. Stromhagen, D. Trines, and B. Willke, "Any light particle search II—technical design report," J. Instrum. **8**, T09001 (2013).
14. M. Meyer, D. Horns, and M. Raue, "First lower limits on the photon-axion-like particle coupling from very high energy gamma-ray observations," Phys. Rev. D **87**, 035027 (2013).
15. M. Giannotti, I. Irastorza, J. Redondo, and A. Ringwald, "Cool WISPs for stellar cooling excesses," J. Cosmol. Astropart. Phys. **2016**, 057 (2016).
16. E. Armengaud, D. Attié, S. Basso, P. Brun, N. Bykovskiy, J. Carmona, J. Castel, S. Cebrián, M. Cicoli, M. Civitani, C. Cogollos, J. Conlon, D. Costa, T. Dafni, R. Daido, A. Derbin, M. Descalle, K. Desch, I. Dratchnev, B. Döbrich, A. Dudarev, E. Ferrer-Ribas, I. Fleck, J. Galán, G. Galanti, L. Garrido, D. Gascon, L. Gastaldo, C. Germani, G. Ghisellini, M. Giannotti, I. Giomataris, S. Gninenko, N. Golubev, R. Graciani, I. Irastorza, K. Jakovčić, J. Kaminski, M. Krčmar, C. Krieger, B. Lakić, T. Lasserre, P. Laurent, O. Limousin, A. Lindner, I. Lomskaya, B. Lubsandorzhiev, G. Luzón, M. C. D. Marsh, C. Margalejo, F. Mescia, M. Meyer, J. Miralda-Escudé, H. Mirallas, V. Muratova, X. Navick, C. Nones, A. Notari, A. Nozik, A. O. de Solórzano, V. Pantuev, T. Papaevangelou, G. Pareschi, K. Perez, E. Picatoste, M. Pivovaroff, J. Redondo, A. Ringwald, M. Roncadelli, E. Ruiz-Chóliz, J. Ruz, K. Saikawa, J. Salvadó, M. Samperiz, T. Schiffer, S. Schmidt, U. Schneekloth, M. Schott, H. Silva, G. Tagliaferri, F. Takahashi, F. Tavecchio, H. ten Kate, I. Tkachev, S. Troitsky, E. Unzhakov, P. Vedrine, J. Vogel, C. Weinsheimer, A. Weltman, and W. Yin, "Physics potential of the international axion observatory (IAXO)," J. Cosmol. Astropart. Phys. **2019**, 047 (2019).
17. LIGO Scientific Collaboration and Virgo Collaboration, "GW150914: the advanced LIGO detectors in the era of first discoveries," Phys. Rev. Lett. **116**, 131103 (2016).
18. Virgo Collaboration, "Advanced virgo: a second-generation interferometric gravitational wave detector," Classical Quantum Gravity **32**, 024001 (2014).
19. LIGO Scientific Collaboration and Virgo Collaboration, "Observation of gravitational waves from a binary black hole merger," Phys. Rev. Lett. **116**, 061102 (2016).
20. LIGO Scientific Collaboration and Virgo Collaboration, "GW170817: observation of gravitational waves from a binary neutron star inspiral," Phys. Rev. Lett. **119**, 161101 (2017).
21. F. Hoogeveen and T. Ziegenhagen, "Production and detection of light bosons using optical resonators," Nucl. Phys. B **358**, 3–26 (1991).
22. G. Mueller, P. Sikivie, D. B. Tanner, and K. van Bibber, "Detailed design of a resonantly enhanced axion-photon regeneration experiment," Phys. Rev. D **80**, 072004 (2009).

23. C. Albrecht, S. Barbanotti, H. Hintz, K. Jensch, R. Klos, W. Maschmann, O. Sawlanski, M. Stolper, and D. Trines, "Straightening of superconducting HERA dipoles for the any-light-particle-search experiment ALPS II," arXiv:2004.13441 (2020).
24. J. H. Põld and A. D. Spector, "Demonstration of a length control system for ALPS II with a high finesse 9.2 m cavity," EPJ Tech. Instrum. **7**, 1–9 (2020).
25. M. T. Hartman, A. Lindner, R. C. G. Smith, A. D. Spector, L.-W. Wei, K. Karan, J. H. Põld, B. Wilke, M. Diaz Ortiz, J. Gleason, A. Hallal, H. Hollis, T. Kozlowski, G. Messineo, G. Mueller, D. B. Tanner, H. Grote, and A. James, "Design of the ALPS II Optical System" (in preparation).
26. J. Dreyling-Eschweiler, N. Bastidon, B. Döbrich, D. Horns, F. Januschek, and A. Lindner, "Characterization, 1064 nm photon signals and background events of a tungsten TES detector for the ALPS experiment," J. Mod. Opt. **62**, 1132–1140 (2015).
27. Z. R. Bush, S. Barke, H. Hollis, A. D. Spector, A. Hallal, G. Messineo, D. B. Tanner, and G. Mueller, "Coherent detection of ultraweak electromagnetic fields," Phys. Rev. D **99**, 022001 (2019).
28. R. Drever, J. Hall, F. Kowalski, J. Hough, G. Ford, A. Munley, and H. Ward, "Laser phase and frequency stabilization using an optical resonator," Appl. Phys. B **31**, 97–105 (1983).
29. E. D. Black, "An introduction to Pound–Drever–Hall laser frequency stabilization," Am. J. Phys. **69**, 79–87 (2001).
30. D. Z. Anderson, "Alignment of resonant optical cavities," Appl. Opt. **23**, 2944–2949 (1984).
31. W. B. Joyce and B. C. DeLoach, "Alignment of Gaussian beams," Appl. Opt. **23**, 4187–4196 (1984).
32. P. Kwee, F. Seifert, B. Willke, and K. Danzmann, "Laser beam quality and pointing measurement with an optical resonator," Rev. Sci. Instrum. **78**, 073103 (2007).
33. S. Kulkarni, A. Umińska, J. Gleason, S. Barke, R. Ferguson, J. Sanjuán, P. Fulda, and G. Mueller, "Ultrastable optical components using adjustable commercial mirror mounts anchored in a ULE spacer," Appl. Opt. **59**, 6999–7003 (2020).
34. F. Cleva, J.-P. Coulon, and M. Merzougui, Virgo Technical Note, VIR-0140A-13, 2013, available at https://tds.virgo-gw.eu/ql/?c=9486.
35. L.-W. Wei, "High-power laser system for Advanced Virgo gravitational wave detector: coherently combined master oscillator fiber power amplifiers," Ph.D. dissertation, (Université Nice Sophia Antipolis, 2015), https://tel.archives-ouvertes.fr/tel-01284969.
36. A. E. Siegman, *Lasers* (University Science Books, 1986).